Journal of Materials Chemistry C

Materials for optical, magnetic and electronic devices

rsc.li/materials-c

ROYAL SOCIETY OF CHEMISTRY
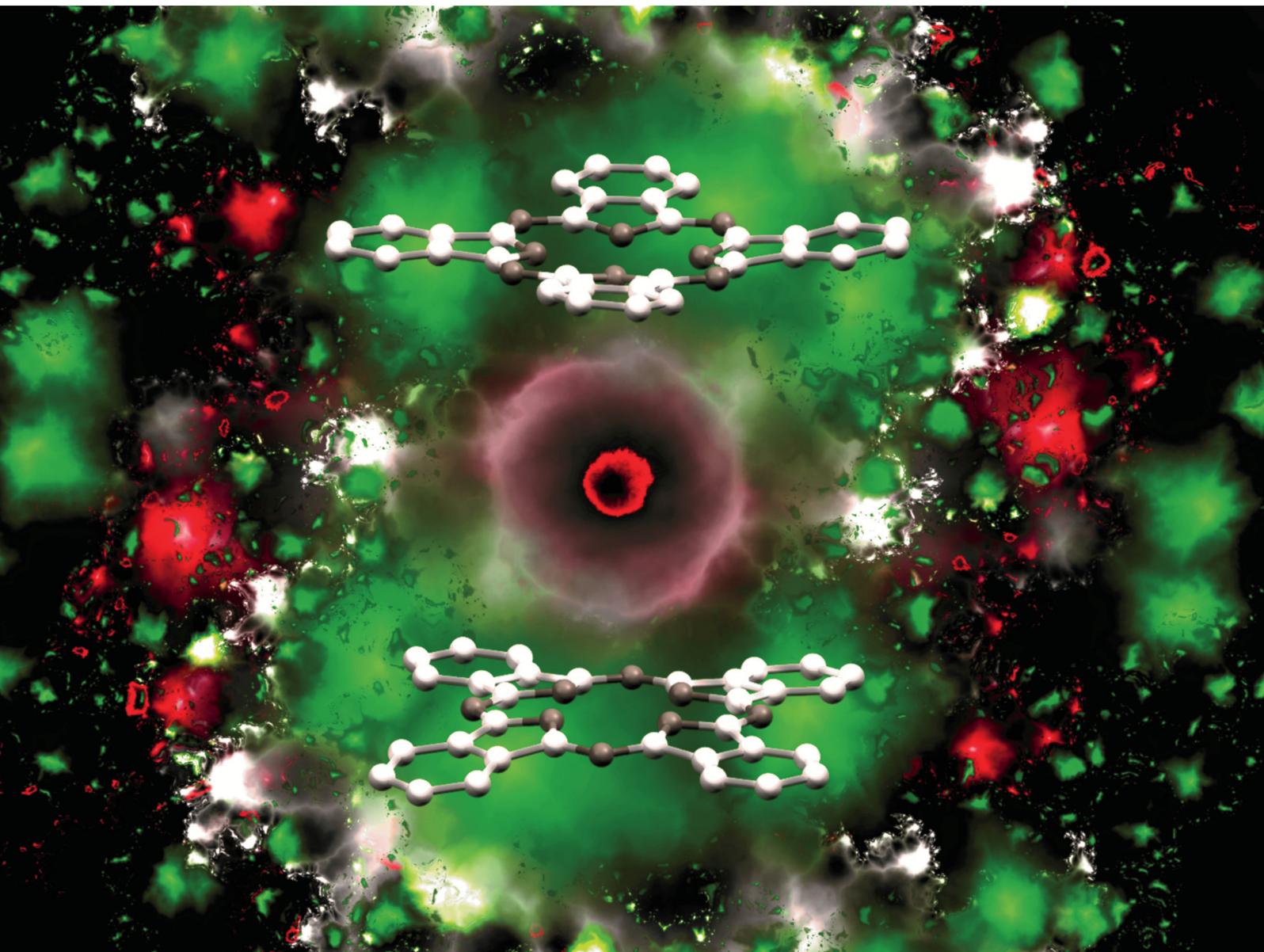
PAPER
Giulia Serrano, Lorenzo Poggini *et al.*
A TbPc₂ sub-monolayer deposit on a titanium dioxide
ultrathin film: magnetic, morphological, and chemical
insights

PAPER

Check for updates

A TbPc₂ sub-monolayer deposit on a titanium dioxide ultrathin film: magnetic, morphological, and chemical insights†

Andrea Luigi Sorrentino, [ID] ab Irene Cimatti,b Giulia Serrano, [ID] *ab
Lorenzo Poggini, [ID] *bc Brunetto Cortigiani,b Luigi Malavolti,de Edwige Otero,f
Philippe Sainctavit,fg Matteo Mannini, [ID] b Roberta Sessoli [ID] b and Andrea Caneschi [ID] a

Thin inorganic films (*i.e.*, metal oxides) are often used as decoupling layers to optimize the interactions between the magnetic layers of molecules and metallic surfaces. For deposits of single-molecule magnets (SMMs), a decoupling layer can minimise the hybridization of the metallic substrate that is responsible for the quenching of their typical magnetic bistability. Here, we explored the potential of a single layer of titania to be used as a decoupling layer, which could represent an interesting playground for widespread use in many technological applications. We used a TiO₂ monolayer with a lepidocrocite-like structure grown on a Ag(100) substrate for the deposition of the terbium(III) bis-phthalocyaninato (TbPc₂) complex. A multi-technique approach employing X-ray photoelectron spectroscopy and scanning tunnelling microscopy was used to examine the integrity of a TbPc₂ sub-monolayer deposit and to study the molecular adsorption configuration on the TiO₂ film. Furthermore, X-ray magnetic circular dichroism was used to investigate the magnetic properties of the TbPc₂ sub-monolayer, revealing that the TiO₂ film successfully preserves the molecular spin character. X-ray-based magnetic measurements showed that the quantum tunnelling of the magnetization characterizing a bulk of molecules is still present and that the present titania film displays a decoupling effect of comparable efficiency to that of a graphene layer.

Introduction

Molecular spintronics is a growing research field focusing on developing innovative devices for sensing, data storage, and quantum applications by combining the properties of inorganic and organic materials.[1,2] In the last few years, single-molecule magnets (SMMs) have aroused significant interest for their use as magnetic building blocks in spintronic micro-devices and

nano-devices[3–7] due to their low-temperature magnetic bistability[8] and unique quantum behaviour.[9] Among systems showing the SMM behaviour, the terbium(III) bis-phthalocyaninato (TbPc₂) neutral complex, consisting of a Tb^III ion coordinated by two phthalocyanine ligands staggered by about 45° with respect to each other,[6,7,10–12] is considered as a perfect candidate for testing these perspectives because of its slow magnetization dynamics at liquid helium temperatures.[13] Besides, its molecular nature allows the formation of monolayer and sub-monolayer deposits on a solid surface. In bulk, the magnetic behaviour of TbPc₂ is dominated by a strong uniaxial anisotropy with the easy axis of magnetization located perpendicular to the Pc rings. The large energy separation between the ground doublet ($J_z = \pm 6$) and the first excited state is responsible for the magnetic bistability as an effective barrier of several hundreds of kelvin opposes the reversal of the magnetization.[14] However, when assembled on different substrates, its magnetism can be highly influenced by the substrate.[15–19] The planar structure of the double-deckers strongly favours a strong electronic interaction with the surface through the π-electrons of the ligands. In particular, a significant quenching of the magnetic bistability in sub-monolayer films assembled on bare metal surfaces has been reported.[17,20–23] In contrast, it has been demonstrated that

a DIEF – Department of Industrial Engineering and INSTM Research Unit, University of Florence, Via S. Marta 3, I-50139 Florence, Italy. E-mail: giulia.serrano@unifi.it

b DICUS – Department of Chemistry "Ugo Schiff" and INSTM Research Unit, University of Florence, I-50019 Sesto Fiorentino (FI), Italy

c ICCOM-CNR, via Madonna del Piano 10, 50019 Sesto Fiorentino, Italy. E-mail: lpoggini@iccom.cnr.it

d Institute for Functional Matter and Quantum Technologies, University of Stuttgart, 70569 Stuttgart, Germany

e Max Planck Institute for Solid State Research, 70569 Stuttgart, Germany

f Synchrotron SOLEIL, L'Orme des Merisiers, Saint Aubin, France

g IMPMC, UMR7590 CNRS, Sorbonne Université, MNHN, Paris, France

† Electronic supplementary information (ESI) available: Additional XPS data and analysis; LEED images and simulations; STM images. See DOI: 10.1039/d1tc03408a

This journal is © The Royal Society of Chemistry 2021

J. Mater. Chem. C, 2021, **9**, 15011–15017 | **15011**

decoupling layers (*e.g.*, graphene or a MgO thin film) can reduce this effect.[19,24–27] Indeed, according to Wäckerlin *et al.*,[27] using a single layer of MgO is not sufficient to efficiently decouple the TbPc$_2$ molecule from a metal substrate. Increasing the MgO layer thickness up to 5 monolayers (ML) improves the magnetic bistability, and TbPc$_2$ features a large magnetic remanence at variance with the butterfly-shaped hysteresis loop observed in the bulk phase.[27,28] The mechanisms behind these substantial changes of SMM properties are still unclear. It has been suggested that the low phonon dispersion of the metal oxide could be a key ingredient for the observation of this enhancement.[28] Furthermore, the possibility of a charge transfer to/from the substrate can affect the crystal field splitting acting on the terbium(III) ion and induce a slower magnetic relaxation.[16]

To obtain further insights on this topic, we investigated the use of an ultrathin film of titanium dioxide (TiO$_2$) grown as a single layer on the Ag(100) surface as an alternative substrate for TbPc$_2$ SMMs.[29] The deposition of atoms and molecules on TiO$_2$ surfaces was already deeply investigated in light of the high surface reactivity of titania surfaces due to the presence of active catalytic sites as surface defects.[30,31] In particular, the deposition of metallated phthalocyanine MPc systems on a bulk TiO$_2$ substrate showed that molecules in direct contact with the surface interact strongly and can undergo an oxidation process.[31–34] Furthermore, our recent studies on bulk TiO$_2$ single crystals revealed that also the sub-monolayer of TbPc$_2$ molecules deposited on the TiO$_2$(110) rutile surface undergoes a strong interfacial interaction independently of the surface preparation and the presence of surface defects.[35]

In this work, we studied the molecular organization and the magnetic properties of a sub-monolayer of TbPc$_2$ molecules thermally sublimated on a TiO$_2$ film grown with a lepidocrocite-like structure on Ag(100) (TiO$_2$-L). Using X-ray photoelectron spectroscopy (XPS) and scanning tunnelling microscopy (STM), we evaluated the presence of intact molecules and their organization on the surface. Finally, by using synchrotron-based X-ray absorption spectroscopy, we evaluated the structural and magnetic properties of the sub-monolayer molecular deposit, confirming the lying-down absorption of the molecules and evidencing the persistence at 2.0 K of the SMM behaviour.

Experimental

The Ag(100) single crystal was cleaned by several cycles of Ar$^+$ sputtering (1500 eV) and annealing (770 K for 30 min) in UHV before the TiO$_2$ film growth. Titanium was subsequently deposited by a Ti (99.999%) rod using an electron beam source. The deposition rate was evaluated by XPS and STM measurements. The TiO$_2$ thin film formation was achieved by depositing the metal under an oxygen partial pressure of 2×10^{-6} mbar in consecutive steps according to the procedure reported in ref. 29 and 36. After the film deposition, the sample was annealed up to 770 K for one hour. The epitaxial growth of the TiO$_2$ thin film on Ag(100) was confirmed by low-energy electron diffraction (LEED). The chemical composition and morphology were

confirmed by XPS and STM measurements, providing results that are in line with previous reports.[29,36] The sublimation of TbPc$_2$ was carried out in a UHV chamber equipped with a home-made Knudsen cell filled with TbPc$_2$ powders. XPS data were acquired using monochromatic Al Kα radiation ($h\nu$ = 1486.6 eV, SPECS mod. XR-MS focus 600) operating at a power of 100 W (13 kV and 7.7 mA) and a SPECS Phoibos 150 1DLD electron analyser mounted at 54.44° to the X-ray source. The XPS spectra were collected at normal emission with the fixed pass energy set to 40 eV. The spectra were analysed using the CasaXPS software. All the spectra were calibrated at the Ti 2p$_{3/2}$ signal at 459.3 eV. The background in the spectra was subtracted using a linear background, and the deconvolution of the XPS spectra was carried out as a combination of Gaussian and Lorentzian functions (70/30).[35] LEED patterns were acquired using an Omicron NG-LEED setup, and the simulation pattern was obtained using the software LEEDPat42.[37]

STM measurements were carried out using an Omicron VT-STM at room temperature for TiO$_2$ characterization and at 35 K for the characterization of TbPc$_2$ deposits. All the images were acquired using an electrochemically etched W tip. Sample preparation and investigation by using XPS, LEED and STM were performed *in situ* with the multi-technique platform available in our laboratory. The TbPc$_2$ deposition has thus been repeated at the synchrotron using the UHV preparation chamber present at the DEIMOS beamline in vacuum connection with the XAS end station. The molecular deposition was performed using the same Knudsen cell used for in-house experiments and operating under similar geometrical and physical conditions. The TiO$_2$-L substrate was prepared in Florence (Italy) and transferred to the DEIMOS beamline facility in Paris (France) using an HV suitcase (with a base pressure of about 10^{-6} mbar).

X-Ray absorption spectroscopy (XAS) experiments were performed at the DEIMOS beamline[38] (SOLEIL synchrotron, Paris), employing both linear and circular polarization and total electron yield (TEY) detection.[39] The investigated temperatures were 4.2 ± 0.2 and 2.0 ± 0.2 K. All the XAS spectra were acquired at B = 3 T at the Tb M$_{4,5}$ edges and the θ parameter was defined as the angle between the k X-ray propagation vector and the normal n to the surface that always lies in the horizontal plane. The X-ray natural linear dichroism (XNLD) was extracted for θ = 45° as the difference between the horizontally (σ^H) and vertically (σ^V) polarized light. The XNLD contribution was normalized with respect to the M$_5$ edge maximum of the isotropic spectrum at θ = 45° $(1/3\sigma^V + 2/3\sigma^H)$ and expressed in percentage (% XNLD).[40] XNLD was not measured at θ = 0° since no signal was expected for any orientation of the molecules because, at the macroscopic scale, there is always a cylindrical symmetry in the plane. X-ray magnetic circular dichroism (XMCD) was measured at θ = 0° as the difference between the XAS spectra obtained using circularly polarized light $(\sigma^- - \sigma^+)$, normalized to the M$_5$ edge maximum of $(\sigma^+ + \sigma^-)/2$ and expressed in percentage (% XMCD). Finally, the magnetic hysteresis curves were obtained by monitoring the field dependence of % XMCD at the Tb M$_5$ edge (1237 eV).

15012 | *J. Mater. Chem. C*, 2021, **9**, 15011–15017

This journal is © The Royal Society of Chemistry 2021

Results and discussion

The TiO$_2$-L film growth was studied by XPS to confirm the expected film stoichiometry[29] and the Ti oxidation state, while STM was used to confirm its quality and morphology. The Ti 2p and O 1s XPS core level spectra are presented in Fig. 1a (top panel) and Fig. S1 (ESI†) (top panel), respectively. Concerning the Ti 2p region, the main Ti^{IV} component (filled in yellow) was accompanied by a small contribution attributed to Ti^{III} sites (filled in green).[41,42] The semi-quantitative analysis of the film (Table S1, ESI†) gave a Ti/O ratio of about 0.4, reflecting a slight excess of oxygen on the surface.[29] Additional details about the XPS characterization can be found in the XPS section of the ESI.† The lepidocrocite structure of the achieved deposit was confirmed by a LEED pattern (Fig. 2a), showing the presence of the TiO$_2$-L structure (red rectangles) on the Ag(100) surface (dashed black square) (see Fig. S2 of the ESI† for details about the LEED analysis). The STM analysis (Fig. 2b and Fig. S3a, ESI†) confirmed the presence of TiO$_2$ islands covering about 80% of the Ag(100) surface. TiO$_2$ islands showed a height of about 0.4 nm (Fig. S3b, ESI†), as previously reported for a single layer of TiO$_2$ with a lepidocrocite-like structure, TiO$_2$-L.[29,43] TiO$_2$ islands featured alternating bright and dark stripes due to the lattice mismatch between the film and the silver surface

lattice (see Fig. 2b).[29] The observed TiO$_2$-L corrugation had the expected periodicity of 10 nm and a height modulation of 0.05 nm. The narrow dark stripes are due to a compression of the oxide layer along the short side of the unit cell, which coincides with the Ag(100) lattice parameters, while the wider bright patches correspond to the unstrained film.[29] The low roughness of the investigated sample further confirms the sub-monolayer nature of the TiO$_2$ film. In fact, thicker deposits lead to non-uniform Stranski–Krastanov growth on Ag(100).[36] As non-ordered 3D islands appear under these conditions, the growth was limited to the first TiO$_2$ layer. A sub-monolayer of TbPc$_2$ (see the inset of Fig. 1b, bottom panel) was sublimated on TiO$_2$-L according to the procedure reported in the Experimental section. Fig. 1b (bottom panel) shows the XPS spectrum of the C 1s core level of the TbPc$_2$ sub-monolayer deposit. The spectrum was fitted using four components. The main one, located at 284.3 eV (filled in grey), was ascribed to the C–C bonds of the phthalocyanine (Pc) ligand, while the second one at 285.5 eV (filled in blue) was ascribed to the C–N bonds of the Pc rings; two satellites (filled in grey and blue) were found at 287.0 eV and 288.1 eV, respectively, which were attributed to C–C and C–N shake-up contributions.[16,44] Due to the overlapping between the N 1s and Ag 3d XPS signals and between the Tb 3d and C KLL plus Ag MNN Auger signals, a semi-quantitative elemental analysis of the molecular layer was not affordable. However, the analysis of the C 1s region indicated a TbPc$_2$ deposit weakly interacting with the substrate.[16,35,45] This is at variance with previous findings for TbPc$_2$ or phthalocyanine molecules in direct contact with a bulk TiO$_2$ substrate where oxidation of the molecular species was observed.[31–35] Such a difference in the substrate reactivity could be an indication of the absence of catalytic sites characteristic of many TiO$_2$ surfaces, such as oxygen vacancies,[30,31] or it can be attributed to a different intrinsic reactivity of the TiO$_2$ lepidocrocite structure compared to the rutile phase used in our previous investigation.[35,46] We notice that also the Ti 2p and O 1s spectra collected after the TbPc$_2$ deposition (Fig. 1a and Fig. S1 (ESI†), bottom panels) do not reveal significant variations in both the line shape and the semi-quantitative analysis (Table S1, ESI†), thus confirming the innocent role played by the TiO$_2$ layer on the assembled molecules. Fig. 2c shows a low-temperature STM image of TbPc$_2$ molecules covering about 10% of TiO$_2$-L islands on Ag(100). After molecular deposition, the corrugated lepidocrocite-like structure[29] is still visible (see the profile in Fig. S4, ESI†), confirming that the TbPc$_2$ absorption did not alter the TiO$_2$ surface. The small-scale STM images of TbPc$_2$ molecules adsorbed on TiO$_2$-L are presented in Fig. 2d and e. TbPc$_2$ molecules show their typical four-lobed features in agreement with previous reports on other surfaces,[15,18,23] indicating a lying down configuration (Pc planes parallel to the surface), as observed on metals and metal oxides.[18,19,21,23] The STM line profiles (the inset in Fig. 2e) reveal that the TbPc$_2$ molecules have an apparent height of 0.30 ± 0.05 nm and a lateral dimension of 2.5 ± 0.1 nm in agreement with previous reports about single TbPc$_2$ molecules on metals.[23,47] It is worth noting that molecules do not pack in
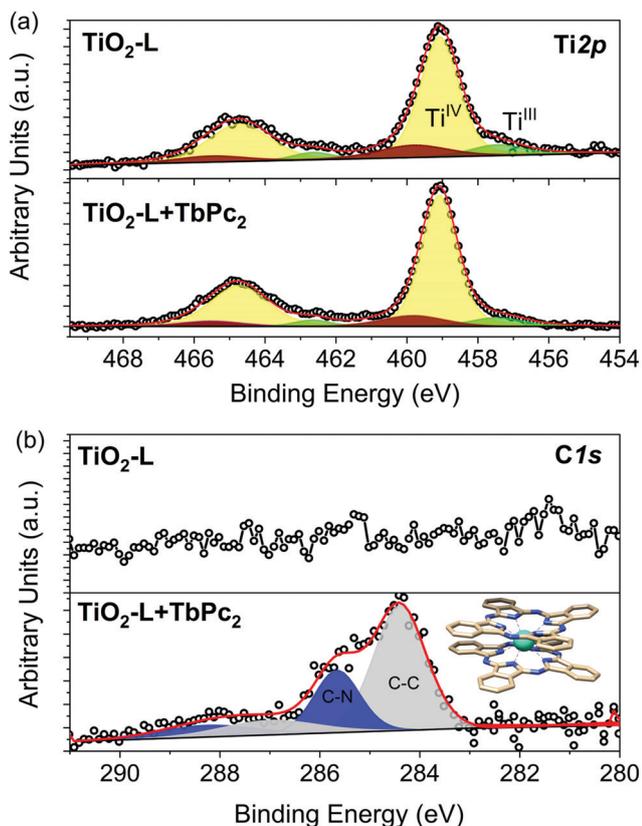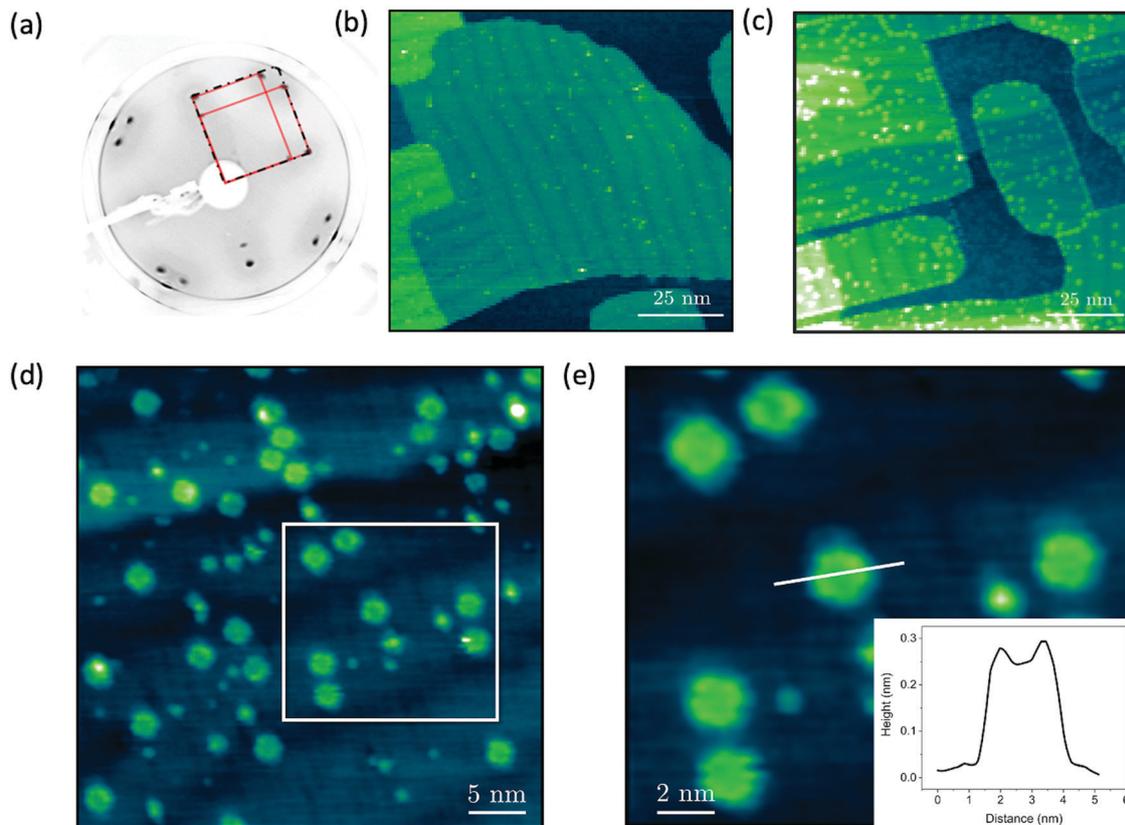

Fig. 1 XPS spectra of (a) Ti 2p and (b) C 1s with the relative deconvolution components before (top panel) and after (bottom panel) the TbPc$_2$ thermal deposition on the TiO$_2$-L substrate. The TbPc$_2$ structure is shown in the inset.

This journal is © The Royal Society of Chemistry 2021

J. Mater. Chem. C, 2021, 9, 15011–15017 | 15013

Fig. 2 (a) LEED pattern of the TiO_2-L surface before the thermal deposition of molecules and (b) its relative STM image (100 pA, 2 V, 150 nm × 150 nm). (c–e) STM images of $TbPc_2$ sublimated on TiO_2-L: (c) large-scale image (20 pA, 2 V, 150 nm × 150 nm); (d) medium scale image (20 pA, 2 V, 40 nm × 40 nm) and (e) its magnification image (20 pA, 2 V, 20 nm × 20 nm) showing a line profile on a single $TbPc_2$ molecule (inset).

regular islands[19,27,47,48] but lie isolated with a random distribution on the TiO_2-L surface, similar to what was observed on Cu(100)[21,23] and for CoPc molecules on TiO_2(100).[32] On the bare Ag(100) areas, small features attributable to phthalocyanines were observed (Fig. S5, ESI†). Their presence may result from (i) a partial thermal decomposition occurring during the deposition process[47,49,50] or (ii) a partial fragmentation of the $TbPc_2$ complex on Ag(100) in the proximity of the reactive TiO_2-L step edges.[51,52]

Low-temperature XAS studies were carried out on the $TbPc_2$ sub-monolayer on TiO_2-L to evaluate the structural and magnetic properties of the molecular layer. The linear and circularly polarized absorption spectrum was recorded at the Tb $M_{4,5}$ edge. The XNLD spectrum (Fig. 3a) revealed a strong negative dichroic signal at 1237 eV, confirming the preferential lying-down configuration of the $TbPc_2$ monolayer[16,17,19,20,27] observed by STM. The XMCD signal (Fig. 3b) measured at 2 K confirmed the characteristic M_5 edge dichroic signal of TbIII ions located at 1237 eV. Dichroism was found to be ca. 135%, in agreement with previous results obtained for the $TbPc_2$ thin film with a similar absorption geometry.[16,17,19,20,27] Indeed, the shape of the XMCD spectrum revealed the presence of a saturated Tb^{III} system characterized by $J = L + S = 6$ total angular momentum.[15,20] Finally, hysteresis loops were recorded at the maximum signal of XMCD (see the Experimental section) at

4.2 K (Fig. 3c) and 2.0 K (Fig. 3d). At 4.2 K, a hysteretic behaviour was substantially absent, at variance with the bulk phase,[53] while the opening of the hysteresis loop was observed at a lower temperature of 2.0 K. The hysteretic behaviour can be better appreciated by looking at the $\Delta_{XMCD}(H)$ value obtained by plotting the difference of the XMCD signal of the up and down branches of the hysteresis loops, $\Delta_{XMCD}(H) = XMCD(H\uparrow) - XMCD(H\downarrow)$ (Fig. S6a, ESI†). This result indicates that the magnetic bistability at 2.0 K is preserved, thus confirming that the TiO2-L film causes an effective decoupling from the metal substrate.[15,27] On the other hand, the observed typical butterfly shape of the magnetic hysteresis loop (Fig. 3d) suggests that the quantum tunnelling of magnetization is not suppressed, similarly to what was reported for other bi-dimensional materials such as graphite[26] and graphene,[19] but at variance with the behaviour observed on MgO films where large magnetic remanence was observed.[27,28] However, a direct comparison with the more efficient decoupling performed by MgO layers cannot be made due to the different thicknesses of the films investigated.[27,29] Indeed, studies on MgO multilayer films (up to 6 ML) showing an increase of the magnetic remanence of $TbPc_2$ also revealed the suppression of conduction electrons scattering from the metal to the molecule.[27] Additionally, we cannot exclude that the partially negative charge of the lepidocrocite-like ultrathin film[36,54] might also influence the
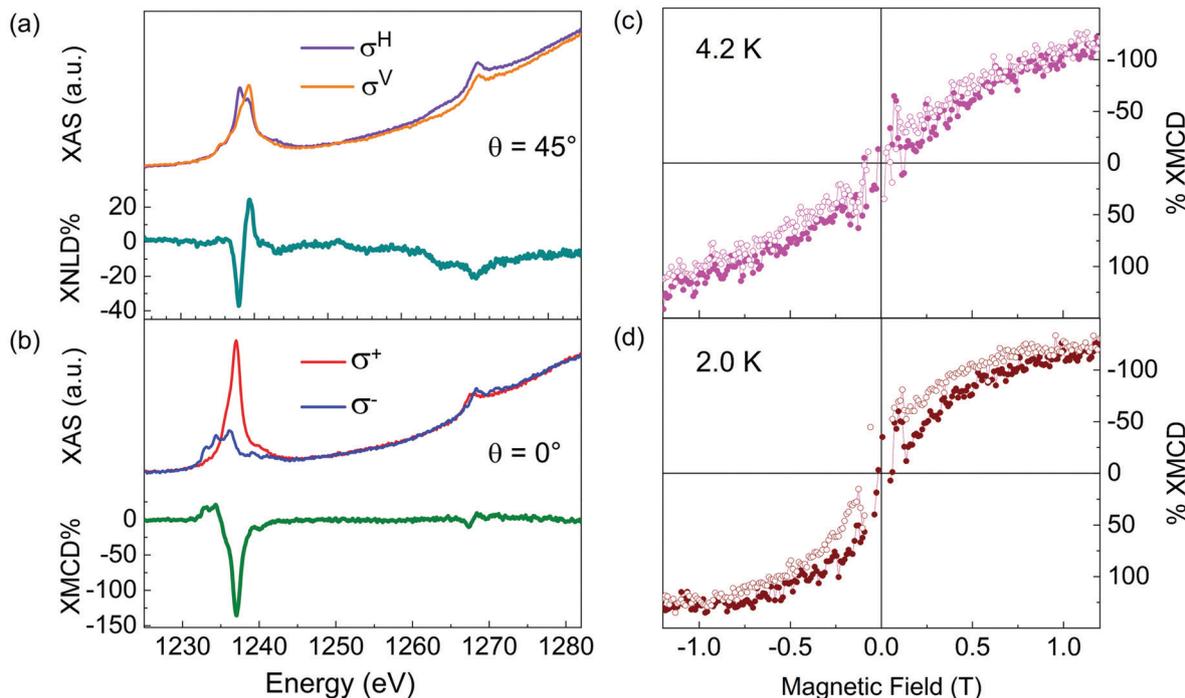
15014 | *J. Mater. Chem. C*, 2021, **9**, 15011–15017

This journal is © The Royal Society of Chemistry 2021

Fig. 3 Magnetic characterisation of the TbPc$_2$ sub-monolayer on the TiO$_2$-L substrate. (a) XAS (top) and XNLD (bottom) spectra recorded at θ = 45°, B = 3 T, and T = 4.2 K. (b) XAS (top) and XMCD (bottom) spectra recorded at θ = 0°, B = 3 T, and T = 4.2 K. The magnetic hysteresis loop recorded at the M$_5$ Tb edge at (c) 4.2 K and (d) 2.0 K with a scan rate of 0.03 T s^{-1}.

electronic distribution of a TbPc$_2$ deposit, causing an alteration of the SMM magnetization dynamics from the bulk behaviour.

Conclusions

XPS and STM measurements showed the integrity of TbPc$_2$ molecules after the thermal deposition on TiO$_2$-L. The STM images indicated a high absorption affinity of this SMM with TiO$_2$, resulting in isolated and randomly distributed molecules. Furthermore, the STM images and XNLD spectra indicated a preferential lying-down configuration of the TbP$_2$ molecules on the TiO$_2$-L structure. The XMCD spectrum shows a marked dichroic signal revealing the maintenance of a Tb^{III} system with an easy axis of magnetization perpendicular to the surface. A butterfly-shaped hysteresis loop was observed at 2.0 K without the suppression of the QTM process, similarly to what was previously observed on graphene. Further, local probe-based spectroscopic experiments combined with theoretical modelling could shed further light on the surface interaction and on the magnetism of TbPc$_2$ on TiO$_2$ thin films to clarify the role of the surface in the suppression or persistence of the SMM behaviour.[55,56] Our results confirmed that ultra-thin layers of decoupling oxides can be used to engineer the interactions between SMMs and metallic substrates.

Author contributions

A. L. S., I. C., G. S., M. M., and B. C. designed the film architecture. A. L. S., I. C., and G. S. prepared the molecular

and oxide deposits and performed the in-house experiments. A. L. S., I. C., G. S, L. P., M. M., R. S., A. C., L. M., E. O., and P. S. designed, performed, and discussed the synchrotron experiments. G. S., L. P. and M. M. drafted the manuscript. M. M., R. S., and A. C. supervised the work. All authors have contributed to and approved the final version of the manuscript.

Conflicts of interest

There are no conflicts to declare.

Acknowledgements

Notes and references

1 S. Sanvito, *Chem. Soc. Rev.*, 2011, **40**, 3336–3355.
2 A. Cornia and P. Seneor, *Nat. Mater.*, 2017, **16**, 505–506.
3 G. Cucinotta, L. Poggini, A. Pedrini, F. Bertani, N. Cristiani, M. Torelli, P. Graziosi, I. Cimatti, B. Cortigiani, E. Otero,

This journal is © The Royal Society of Chemistry 2021

J. Mater. Chem. C, 2021, **9**, 15011–15017 | **15015**

R. Sessoli, M. Mannini, P. Ohresser, P. Sainctavit, A. Dediu, E. Dalcanale, R. Sessoli and M. Mannini, *Adv. Funct. Mater.*, 2017, **27**, 1703600.

4 M. Urdampilleta, N. V. Nguyen, J. P. Cleuziou, S. Klyatskaya, M. Ruben and W. Wernsdorfer, *Int. J. Mol. Sci.*, 2011, **12**, 6656–6667.

5 A. Candini, S. Klyatskaya, M. Ruben, W. Wernsdorfer and M. Affronte, *Nano Lett.*, 2011, **11**, 2634–2639.

6 R. Vincent, S. Klyatskaya, M. Ruben, W. Wernsdorfer and F. Balestro, *Nature*, 2012, **488**, 357–360.

7 L. Bogani and W. Wernsdorfer, *Nat. Mater.*, 2008, **7**, 179–186.

8 G. Christou, D. Gatteschi, D. N. Hendrickson and R. Sessoli, *MRS Bull.*, 2000, 66–71.

9 G. Serrano, L. Poggini, M. Briganti, A. L. Sorrentino, G. Cucinotta, L. Malavolti, B. Cortigiani, E. Otero, P. Sainctavit, S. Loth, F. Parenti, A.-L. L. Barra, A. Vindigni, A. Cornia, F. Totti, M. Mannini and R. Sessoli, *Nat. Mater.*, 2020, **19**, 546–551.

10 M. Urdampilleta, S. Klyatskaya, J.-P. Cleuziou, M. Ruben and W. Wernsdorfer, *Nat. Mater.*, 2011, **10**, 502–506.

11 S. Thiele, R. Vincent, M. Holzmann, S. Klyatskaya, M. Ruben, F. Balestro and W. Wernsdorfer, *Phys. Rev. Lett.*, 2013, **111**, 037203.

12 M. Urdampilleta, S. Klayatskaya, M. Ruben and W. Wernsdorfer, *ACS Nano*, 2015, **9**, 4458–4464.

13 C. Godfrin, A. Ferhat, R. Ballou, S. Klyatskaya, M. Ruben, W. Wernsdorfer and F. Balestro, *Phys. Rev. Lett.*, 2017, **119**, 187702.

14 N. Ishikawa, M. Sugita, N. Tanaka, T. Ishikawa, S. Koshihara and Y. Kaizu, *Inorg. Chem.*, 2004, **43**, 5498–5500.

15 E. Moreno Pineda, T. Komeda, K. Katoh, M. Yamashita and M. Ruben, *Dalton Trans.*, 2016, **45**, 18417–18433.

16 M. Mannini, F. Bertani, C. Tudisco, L. Malavolti, L. Poggini, K. Misztal, D. Menozzi, A. Motta, E. Otero, P. Ohresser, P. Sainctavit, G. G. Condorelli, E. Dalcanale and R. Sessoli, *Nat. Commun.*, 2014, **5**, 4582.

17 L. Malavolti, L. Poggini, L. Margheriti, D. Chiappe, P. Graziosi, B. Cortigiani, V. Lanzilotto, F. B. de Mongeot, P. Ohresser, E. Otero, F. Choueikani, P. Sainctavit, I. Bergenti, V. A. Dediu, M. Mannini and R. Sessoli, *Chem. Commun.*, 2013, **49**, 11506.

18 G. Serrano, S. Wiespointner-Baumgarthuber, S. Tebi, S. Klyatskaya, M. Ruben, R. Koch and S. Müllegger, *J. Phys. Chem. C*, 2016, **120**, 13581–13586.

19 G. Serrano, E. Velez-Fort, I. Cimatti, B. Cortigiani, L. Malavolti, D. Betto, A. Ouerghi, N. B. Brookes, M. Mannini and R. Sessoli, *Nanoscale*, 2018, **10**, 2715–2720.

20 L. Margheriti, D. Chiappe, M. Mannini, P.-E. Car, P. Sainctavit, M.-A. Arrio, F. B. de Mongeot, J. C. Cezar, F. M. Piras, A. Magnani, E. Otero, A. Caneschi and R. Sessoli, *Adv. Mater.*, 2010, **22**, 5488–5493.

21 S. Stepanow, J. Honolka, P. Gambardella, L. Vitali, N. Abdurakhmanova, T. Tseng, S. Rauschenbach, S. L. Tait, V. Sessi, S. Klyatskaya, M. Ruben and K. Kern, *J. Am. Chem. Soc.*, 2010, **132**, 11900–11901.

22 L. Vitali, S. Fabris, A. M. Conte, S. Brink, M. Ruben, S. Baroni and K. Kern, *Nano Lett.*, 2008, **8**, 3364–3368.

23 Z. Deng, S. Rauschenbach, S. Stepanow, S. Klyatskaya, M. Ruben and K. Kern, *Phys. Scr.*, 2015, **90**, 098003.

24 S. Marocchi, A. Candini, D. Klar, W. Van den Heuvel, H. Huang, F. Troiani, V. Corradini, R. Biagi, V. De Renzi, S. Klyatskaya, K. Kummer, N. B. Brookes, M. Ruben, H. Wende, U. del Pennino, A. Soncini, M. Affronte and V. Bellini, *ACS Nano*, 2016, **10**, 9353–9360.

25 V. Corradini, A. Candini, D. Klar, R. Biagi, V. De Renzi, A. Lodi Rizzini, N. Cavani, U. del Pennino, S. Klyatskaya, M. Ruben, E. Velez-Fort, K. Kummer, N. B. Brookes, P. Gargiani, H. Wende and M. Affronte, *Nanoscale*, 2018, **10**, 277–283.

26 M. Gonidec, R. Biagi, V. Corradini, F. Moro, V. De Renzi, U. del Pennino, D. Summa, L. Muccioli, C. Zannoni, D. B. Amabilino and J. Veciana, *J. Am. Chem. Soc.*, 2011, **133**, 6603–6612.

27 C. Wäckerlin, F. Donati, A. Singha, R. Baltic, S. Rusponi, K. Diller, F. Patthey, M. Pivetta, Y. Lan, S. Klyatskaya, M. Ruben, H. Brune and J. Dreiser, *Adv. Mater.*, 2016, **28**, 5195–5199.

28 M. Studniarek, C. Wäckerlin, A. Singha, R. Baltic, K. Diller, F. Donati, S. Rusponi, H. Brune, Y. Lan, S. Klyatskaya, M. Ruben, A. P. Seitsonen and J. Dreiser, *Adv. Sci.*, 2019, **6**, 1901736.

29 A. Atrei, A. M. Ferrari, D. Szieberth, B. Cortigiani and G. Rovida, *Phys. Chem. Chem. Phys.*, 2010, **12**, 11587.

30 S. C. Li, L. N. Chu, X. Q. Gong and U. Diebold, *Science*, 2010, **328**, 882–884.

31 S. Yu, S. Ahmadi, P. Palmgren, F. Hennies, M. Zuleta and M. Göthelid, *J. Phys. Chem. C*, 2009, **113**, 13765–13771.

32 N. Ishida and D. Fujita, *J. Phys. Chem. C*, 2012, **116**, 20300–20305.

33 P. Palmgren, K. Nilson, S. Yu, F. Hennies, T. Angot, J. M. Layet, G. Le Lay and M. Gothelid, *J. Phys. Chem. C*, 2008, **112**, 5972–5977.

34 S. Ahmadi, B. Agnarsson, I. Bidermane, B. M. Wojek, Q. Noël, C. Sun and M. Göthelid, *J. Chem. Phys.*, 2014, **140**, 174702.

35 G. Serrano, A. L. Sorrentino, L. Poggini, B. Cortigiani, C. Goletti, R. Sessoli and M. Mannini, *Phys. Chem. Chem. Phys.*, 2021, **23**, 12060–12067.

36 A. Atrei, B. Cortigiani and A. M. Ferrari, *J. Phys.: Condens. Matter*, 2012, **24**, 445005.

37 K.E. Hermann (FHI) and M.A. Van Hove (HKBU), Berlin/ Hong Kong, 2014.

38 P. Ohresser, E. Otero, F. Choueikani, K. Chen, S. Stanescu, F. Deschamps, T. Moreno, F. Polack, B. Lagarde, J.-P. Daguerre, F. Marteau, F. Scheurer, L. Joly, J.-P. Kappler, B. Muller, O. Bunau and P. Sainctavit, *Rev. Sci. Instrum.*, 2014, **85**, 013106.

39 R. Nakajima, J. Stöhr and Y. U. Idzerda, *Phys. Rev. B: Condens. Matter Mater. Phys.*, 1999, **59**, 6421–6429.

40 C. Brouder, *J. Phys.: Condens. Matter*, 1990, **2**, 701–738.

15016 | *J. Mater. Chem. C*, 2021, **9**, 15011–15017

This journal is © The Royal Society of Chemistry 2021

41 M. J. Jackman, A. G. Thomas and C. Muryn, *J. Phys. Chem. C*, 2015, **119**, 13682–13690.

42 A. L. Sorrentino, G. Serrano, L. Poggini, B. Cortigiani, K. E. El-Kelany, M. D'Amore, A. M. Ferrari, A. Atrei, A. Caneschi, R. Sessoli and M. Mannini, *J. Phys. Chem. C*, 2021, **125**, 10621–10630.

43 G. T. Harrison, M. C. Spadaro, C. L. Pang, D. C. Grinter, C. M. Yim, P. Luches and G. Thornton, *Mater. Sci. Technol.*, 2016, **32**, 203–208.

44 Y. Zhang, T. Learmonth, S. Wang, A. Y. Matsuura, J. Downes, L. Plucinski, S. Bernardis, C. O'Donnell and K. E. Smith, *J. Mater. Chem.*, 2007, **17**, 1276.

45 A. Pedrini, L. Poggini, C. Tudisco, M. Torelli, A. E. Giuffrida, F. Bertani, I. Cimatti, E. Otero, P. Ohresser, P. Sainctavit, M. Suman, G. G. Condorelli, M. Mannini and E. Dalcanale, *Small*, 2018, **14**, 1702572.

46 W.-K. Li, X.-Q. Gong, G. Lu and A. Selloni, *J. Phys. Chem. C*, 2008, **112**, 6594–6596.

47 K. Katoh, Y. Yoshida, M. Yamashita, H. Miyasaka, B. K. Breedlove, T. Kajiwara, S. Takaishi, N. Ishikawa, H. Isshiki, Y. F. Zhang, T. Komeda, M. Yamagishi and J. Takeya, *J. Am. Chem. Soc.*, 2009, **131**, 9967–9976.

48 F. Ara, Z. K. Qi, J. Hou, T. Komeda, K. Katoh and M. Yamashita, *Dalton Trans.*, 2016, **45**, 16644–16652.

49 M. Toader, M. Knupfer, D. R. T. Zahn and M. Hietschold, *J. Am. Chem. Soc.*, 2011, **133**, 40.

50 A. Kumar, K. Banerjee and P. Liljeroth, *Nanotechnology*, 2017, **28**, 082001.

51 H. Fei Wen, M. Miyazaki, Q. Zhang, Y. Adachi, Y. Jun Li and Y. Sugawara, *Phys. Chem. Chem. Phys.*, 2018, **20**, 28331.

52 X. Q. Gong and A. Selloni, *J. Catal.*, 2007, **249**, 134–139.

53 L. Malavolti, M. Mannini, P.-E. Car, G. Campo, F. Pineider and R. Sessoli, *J. Mater. Chem. C*, 2013, **1**, 2935.

54 S. Tosoni and G. Pacchioni, *J. Phys. Chem. C*, 2020, **124**, 20960–20973.

55 S. Baumann, W. Paul, T. Choi, C. P. Lutz, A. Ardavan and A. J. Heinrich, *Science*, 2015, **350**, 417–420.

56 W. Paul, K. Yang, S. Baumann, N. Romming, T. Choi, C. P. Lutz and A. J. Heinrich, *Nat. Phys.*, 2017, **13**, 403–407.

This journal is © The Royal Society of Chemistry 2021

J. Mater. Chem. C, 2021, **9**, 15011–15017 | **15017**